Colloids and Surfaces B: Biointerfaces 207 (2021) 112008

Contents lists available at ScienceDirect

Colloids and Surfaces B: Biointerfaces

journal homepage: www.elsevier.com/locate/colsurfb

Augment the efficacy of eradicating metastatic lesions and tumor proliferation in breast cancer by honokiol-loaded pH-sensitive targeted lipid nanoparticles

Hongyan Zhang [a,1], Ji Li [b,1], Rong Yuan [c], Yufen Li [b], Yue Zhang [a], Xiaoyun Hu [a], Jiqiang Qu [c], Yu Chen [a], Zheran Wang [d,*], Mingyu Xia [c,*], Dongkai Wang [a,*]

[a] Department of Pharmaceutics, Shenyang Pharmaceutical University, No. 103, Wenhua Road, Shenyang, China
[b] Department of Traditional Chinese Medicine, Shenyang Pharmaceutical University, No. 103, Wenhua Road, Shenyang, 110016, China
[c] Department of Pharmacology, Shenyang Pharmaceutical University, No. 103, Wenhua Road, Shenyang, 110016, China
[d] Department of Mathematics and Statistics, Auburn University, 221 Parker Hall, Auburn, AL, 36849, United States

ARTICLE INFO

Keywords:
Lipid-polymer hybrid nanoparticles
Honokiol
pH responsive
Metastasis
Breast cancer

ABSTRACT

Functionally-enabled delivery systems for aggressive lung metastases from breast cancer have been broadly examined, and the simultaneous inhibition of metastasis while fighting tumors persists as a provocative concern. We propose a valid strategy for delivering natural drugs-Honokiol (Hol) to achieve eradication of breast cancer cells and inhibition of pulmonary metastasis. A non-toxic degradable pH-sensitive polymer-PBAE for encapsulated Hol, and the outer layer was wrapped with Folate-DSPE-PEG_{2000} (FA/PBAE/Hol-NPs), which have strengthened stability, prolonged *in vivo* circulation time and efficiently targets tumor sites. FA/PBAE/Hol-NPs displayed dampening the capability of migration and invasion, elevated 4T1 uptake and boosted apoptosis. What's more, 4T1 breast cancer model mice exhibited marked anti-tumor (Inhibition rate of 62.8 %) and lung metastasis suppression (Inhibition rate of 84.3 %). In parallel, histological immunofluorescence and immunohistochemical assays demonstrate higher apoptosis levels and repression of matrix metalloproteinase expression in mice, all of which are instrumental in inhibiting lung metastasis. Taken together, FA/PBAE/Hol-NPs can as an efficacious intravenous drug delivery system for the curative treatment of metastatic breast cancer.

1. Introduction

Breast cancer is the most morbid malignancy in females, and the overwhelming clinical consensus is that majority of breast cancer survivors do not survive *in situ* breast cancer, rather they die from tumor metastasis [1–3]. About 2/3 of these breast cancer patients have undergone pulmonary metastasis at the onset of death [4,5]. Accordingly, when treating primary tumors, the prevention of tumor metastasis at the simultaneous time ought to be a priority. To tackle these challenging issues, there have been numerous endeavors to formulate nano drug delivery systems, such as liposomes and micelles for loading chemotherapeutic drugs [6–8]. However, conventional chemotherapeutic drugs have severe side effects and limited therapeutic effect on tumor metastasis [9]. Therefore, it is imperative to select a natural anticancer drug with low cost, low side effects, and easy access to accurately deliver into tumor tissues by appropriately nano delivery system to accomplish the dual effects of efficient elimination of primary tumor and suppression of metastasis. Chinese herb-Honokiol (Hol) is a biphenol naturally occurring chemical compound separated out from the bark and leaves of Magnolia officinalis, its efficacy on several chronic diseases has also been broadly well-studied (gastrointestinal disorders, cough, anxiety, antithrombotic, and antidepressant, *etc.*) [10–12]. Prospectively, in recently years scientists have proven its anti-tumor effectiveness towards breast cancer, lung cancer, and skin and liver cancers [13]. Hol is capable of suppressing tumor invasion and metastasis by inhibition of MMPs, NF-kB, EGFR, PI3K/AKT/mTOR and Ras/ERK pathways [14,15]. Yet, distressingly, the aqueous dissolution and inferior biological availability of Hol restrict its usage in the clinical therapy of cancer. How to devise a novel strategy to conquer the deficiency of Hol is critically important.

* Corresponding authors.
E-mail addresses: zzw0049@auburn.edu (Z. Wang), xmywd@vip.sina.com (M. Xia), wangycsyphu@126.com (D. Wang).
[1] These authors contributed to the work equally.

https://doi.org/10.1016/j.colsurfb.2021.112008
Received 11 May 2021; Received in revised form 16 July 2021; Accepted 24 July 2021
Available online 27 July 2021

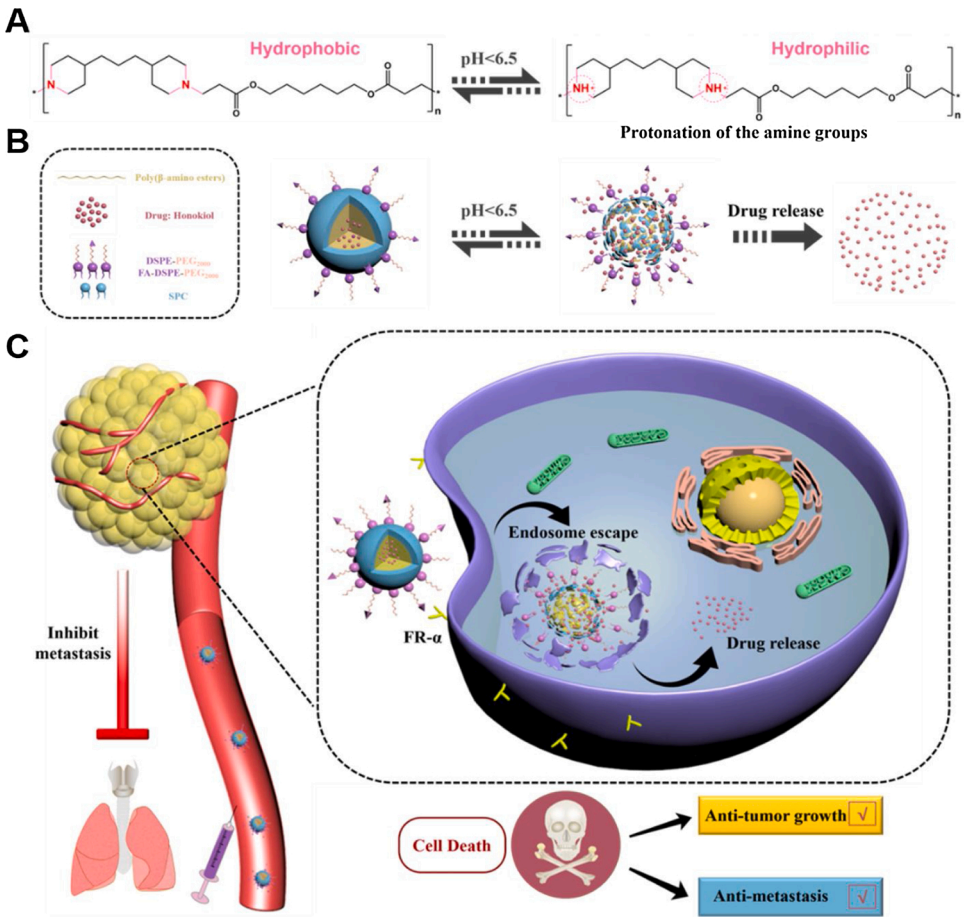

Scheme 1. Abstract concept graphic of FA/PBAE/Hol-NPs can inhibit tumor and metastasis by effectively delivering Hol *in vivo*. (A) The drug release was due to the change of solubility caused by protonation of amino group in PBAE at pH < 6.5; (B) Preparation of FA/PBAE/Hol-NPs; (C) FA/PBAE/Hol-NPs exhibited the effect of anticancer and inhibiting lung metastasis.

It is known that the pH in tumor tissues and endosomes (pH 6.0−5.0) is considerably more acidic in comparison to the physiological (pH 7.4) [16]. The physics of pH-responsive nanocarriers, like swelling/contraction and dissociation and clustering of particles, is responsive to variations in environmental pH [17]. Consequently, the employment of acid-sensitive nanodrug delivery systems is intended to foster tumor-specific drug delivery. A host of polymeric nanodrug delivery systems comprising acid-responsive chemical bonds or functional groups have been conceived to boost tumor therapeutic efficacy targeting the slightly acidic environment of tumor tissues and subcellular organelles within cells [18–20]. Among pH-sensitive polymers, poly (β-amino) ester (PBAE) is widely utilized as a biodegradable and low cytotoxic agent in anti-cancer drug delivery systems. It is protonated at endosomal pH and encourages the escape of encapsulated drugs *via* a "proton sponge" effect [21–23].

Several ligands targeting tumor cell-specific receptors have been conjugated to the surface of NPs to deliver them into the cell through receptor-mediated endocytosis [24]. Of these, folic acid (FA) is a targeting agent that has displayed immense potential in targeted drug delivery systems due to its high binding to the folate receptor (FR), which has been proven to be overexpressed in a broad range of human tumors, including breast cancer, whereas poorly expressed in normal healthy tissues [25]. Once introduced into the physiological environment, nanoparticles (NPs) are instantly wrapped by proteins, resulting in a so-called protein corona with effect on targeting [26,27]. Therefore, it is necessary to select the appropriate target head, particle size as well as PEG length. Certainly, the targeting ability as well as the therapeutic efficacy of FA were well reflected in this study.

In this investigation, lipid-polymer hybrid nanoparticles (LPHNs) with pH-sensitive property were conceived to simultaneous curb breast cancer cell development and metastasis, using PBAE, as the core, and the hydrophobic drug Hol, was encapsulated by hydrophobic interaction. FA target head modification of LPHNs in binding to the receptor overexpressed on 4T1 breast cancer cells FR (Scheme 1). Hol-loaded LPHNs were initially formulated for characterization, and then the cellular uptake, endo/lysosomal escape, and cytotoxic effects of Hol-loaded LPHNs were evaluated. Subsequently, since not much research has been done on Hol and in conjunction with the cytotoxicity of the drug-loaded formulation designed, three concentrations were designed to investigate the inhibition of tumor cell migration and invasion by Hol-loaded LPHNs was addressed *in vitro*. Lastly, its biodistribution in tissues, *in vivo* antitumor potency, and ability to arrest tumor metastasis were estimated on a 4T1 breast tumor model. In summary, research has identified that FA/PBAE/Hol-NPs can improve the solubility of Hol and control the release of drugs on demand, which provides a new chemotherapy prescription for Hol against breast cancer and lung metastasis.

2. Experimental part

2.1. Reagents & procedures

Annexin V-FITC apoptosis detection kit, Honokiol and Lyso-Tracker™ Red were procured from Dalian Meilun Pharmaceutical Technology Co., Ltd. (Dalian, China). TDP, HDD and Coumarine-6 (C6) were acquired from Aladdin Reagent Co., Ltd. (Shanghai, China). MTT and Hoechst 33342 were kindly submitted by Sigma-Aldrich (St. Louis,

MO). DiR was made available by AAT Bioquest Inc (Sunnyvale, CA). All the phospholipids have been sourced from Advanced Vehicle Technology Pharmaceutical Co., Ltd. (Shanghai, China).

2.2. Cells and animals

4T1 breast cancer cells were available from the German DMSZ cell stock. Healthy female BALB/c mice (5–6 weeks old) were sourced from the Experimental Animal Center of Shenyang Pharmaceutical University (Shenyang, China). Animal studies were done in adherence to the guidelines of the Laboratory Animal Center and were authorized by the Animal Ethics Committee of Shenyang Pharmaceutical University with ethical permission No. SYPU-IACUCC2020-11-20-106.

2.3. PBAE synthesis and properties

The details of the synthesis of PBAE were by Michael addition reaction. Determination of the base dissociation constant (pKb) of PBAE by titration with acid-base potentiometric method [28]. Simply, PBAE was solubilized in diluted water with a concentration of 1 mg/mL (a little methanol to assist dissolution). The pH was regulated to approximately 3.0 with HCl solution. The solutions were subsequently titrated with 0.1 M NaOH in 50 μL-100 μL of increments. Among them, the blank control group was normal saline of pH = 3.0, and the rest was proceeded as above. The pH titration curve was plotted in terms of the pH value of the solution.

2.4. Hol-loaded LPHNs preparation work

The Hol-loaded NPs were elaborated by a single emulsion (O/W) solvent evolution technique. 10 mg PBAE and 3 mg Hol were solubilized in 1 mL $CHCl_3$, and 3.3 mg SPC, 3 mg DSPE-PEG_{2000} and FA-DSPE-PEG_{2000} (w/w:9/1) were mixed into 6 mL of aqueous phase (4% ethanol), and the organic phase was gradually incorporated into the aqueous phase through a vortex mixer within 60 s, further vortexed for 60 s. Thereafter, the probe was ultrasonicated in an iced bath (power 300 w, operation 3 s, intermittent operation 2 s, 95 cycles) and the organic solvent was eliminated by rotary evaporation under decreased pressure, when no bubbles occurred in the flask, it was rotated for 20 min to fully eliminate the organic solution to yield a light blue suspension of emulsion lipid polymer mixed nanoparticles.C6 or DiR-loaded LPHNs were manufactured in a manner analogous to that mentioned above. The uncoated Hol of LPHNs were removed by Sephadex G-50 micro-column-centrifugation method. The final Hol-loaded NPs were kept in a freezer at 2–8 ℃.

The HPLC was applied to evaluate the concentration of Hol. The separation was performed on a COSMOSIL column (250 mm × 4.6 mm, 5 μm) at 25 ℃ with a mobile phase of 75:25 v/v mixture of acetonitrile and 0.2 % formic acid water at a flow rate of 1 mL/min. The encapsulation efficiency (EE%) and drug loading capacity (DL%) of Hol-loaded NPs were quantified employing by Sephadex G-50 micro-column-centrifugation method. DL% and EE% were obtained using Eqs. (1) and (2).

$$EE\% = \frac{W_{en}}{W_t} \times 100\% \quad (1)$$

$$DL\% = \frac{W_{en}}{W_t + W_l + W_p} \times 100\% \quad (2)$$

Among them, where W_{en} is the actual measured amount of encapsulated drug, W_t is the gross drug delivery of Hol-loaded NPs, W_l is the aggregate mass of polymer, and W_p is the sum of Hol-loaded LPHNs incorporated with phospholipids.

2.5. The size, zeta potential and morphology profiles of LPHNs

The sizes and zeta potentials of LPHNs were registered employing a dynamic light scattering (DLS) zeta-sizer (Malvern Instruments, Malvern, UK). The morphology was visualized by staining FA/PBAE-NPs and PBAE-NPs with phosphotungstic acid solution (0.2 %, w/v), followed by transmission electron microscopy (TEM). To assess the stability of LPHNs, the particle size was estimated by DLS.

2.6. Superficial charge transition and pH responsiveness of LPHNs

The variation in size and zeta potential of blank LPHNs was ascribed to pH values viewed by DLS at 25 °C: 1 mL of sample was placed in incubation with 5 mL of PBS at varying pH values (7.4 and 5.5) to gauge the particle size, and the zeta potential of blank LPHNs was observed with PBS at varied pH values (pH = 2–10).

2.7. In vitro profile of the release of Hol-loaded LPHNs

The *in vitro* release properties of Hol-loaded LPHNs were evaluated employing a dialysis membrane method. PBS (pH 7.4, pH 6.8 and pH 5.5) and 0.2 % (w/v) Tween-80 were opted as the release medium. Briefly, 1.0 mL (100 mg/mL) of the Hol-loaded nanoparticle solution was disposed into a MWCO = 3500 dialysis pouch. The dialysis bag was shifted to a bottle containing 20 mL of release medium of varying pH and stirred at 37 ± 0.2 °C and 100 rpm. After taking out 1 mL of release medium at a scheduled time and joining the identical amount of blank medium. All samples were performed three times at each pH.

2.8. Solid-state properties

In an attempt to elucidate the existence form of Hol in LPHNs, blank carriers, the physical mixture of free Hol and blank LPHNs (PM), drug carriers and free drugs were subjected by XRD (MiniFlex 600, Rigaku, Japan), DSC (DSC2500, Mettler Toledo, Switzerland) and FTIR (Spectrum 1000, PerkinElmer, USA).

2.8.1. X-ray powder diffraction (XRD)

The crystal architectures of all samples were inspected and optimized using X-ray diffraction. The scope of measurement was 3–50° for each sample. Appropriate processing parameters were: step angle 0.02°, generator electric current 30 mA, generator tensor 40 kV, and scanning speed 4°/min.

2.8.2. Differential scanning calorimetry (DSC)

The thermo properties of all samples were investigated in a DSC apparatus. Samples of 2−5 mg were deposited in a hermetically sealing aluminum tray and thereafter heated from 40 °C to 110 °C taking a 10 °C/min heating ratio in a N_2 atmosphere.

2.8.3. Fourier transform infrared spectroscopy (FTIR)

The FT-IR were utilized to carry out the analyses of the chemical structures of all samples within a 400−4000 cm^{-1} scan interval.

2.9. Uptake and delivery of Hol-loaded NPs in vitro

2.9.1. Cellular uptake

To observe the pH-responsive cellular uptake of Hol-loaded NPs, 4T1 cells were individually seeded for 24 h on microscope slides in a 6-well plate with a density of 3.0×10^4 cells/well and incubated for 12 h in a humidified atmosphere of 5% CO_2 at 37 °C. The cells were administered with C6-loaded NPs at a concentration of 40 μg/mL. After incubation for 2 or 6 h, the cells were rinsed with cold PBS, and then fixed with 4% paraformaldehyde for 10 min. Cell nuclei were stained with Hoechst 33258 (1 μg/mL, 25 min). At last, the cells were immobilized on glass slides and visualized with laser scanning confocal microscopy (CLSM,

ZEISS710, Germany). Folate receptor-mediated endocytosis was examined by assaying the effect of free FA on the intake of FA/PBAE-NPs. 4T1 cells were processed with 1 mM free FA to block folate receptor conjugation for 1 h, and subsequently cells thereafter subjected to C6-FA/PBAE-NPs.

To ascertain the intracellular delivery efficiency of the drug delivering system, the intracellular allocation and trafficking of C6-loaded NPs was also evaluated by CLSM. Lysosomes were colored with LysoTracker Red and nuclei were dyed as described above.

2.9.2. Flow cytometry with in vitro quantitative intake

To quantitatively examine the *in vitro* cellular uptake of Hol in diverse agents by tumor cells, 4T1 cells were seeded on 6-well plates with an intensity of 3×10^4 cell per well and cultured for 24 h. Cells were subsequently processed with C6-loaded NPs, and the fluorescence intensity of C6 was detected by flow cytometry analysis (FC500, Beckman Coulter, USA) following 2 h and 4 h.

2.10. In vitro cytotoxicity studies and apoptotic rate

The cytotoxicity of the Hol-loaded LPHNs was judged *via* MTT assay. 4T1 cells in 96-well panels were cultivated with 1×10^4 cells/well of medium. Overnight cultivation, the cells were treated with free Hol, FA/PBAE/Hol-NPs and PBAE/Hol-NPs at designed concentrations. Cells were incubated for 24 h and then incubated with MTT (5 mg/mL in PBS) for another 4 h at 37 °C. Subsequently, the supernatant was eliminated and the blue formazan crystals solubilized with DMSO (150 μL). Using a microplate reader, the absorbance of each well was taken at 570 nm.

Apoptosis was detectable employing AVPI and flow cytometry. Briefly, 4T1 cells were treated with free Hol, PBAE/Hol-NPs and FA/PBAE/Hol-NPs (Hol equivalent at a level of 2.5 μg/mL) for 24 h during the logarithmic growth phase by inoculation in 6-well plates, 3×10^5 /well. Use untreated cells as a negative control. Add Binding buffer working solution to settle the cells when resuspended, then add 5 μL Annexin V-FITC and PI, mix gently, incubate at room condition without light for 15 min. Eventually detect the apoptotic cells by flow cytometry.

2.11. Transwell migration and Wound-healing migration assay

Chambers (8 μm pore size, Corning, 3422) are being employed to appraise the capability of LPHNs in restraining cell invasion [9]. 4T1 breast cancer cells (4×10^5 cells/mL) were suspension in 200 μL of RPMI-1640 with 1% FBS were incorporated into the upper chamber, RPMI-1640 (500 μL) with 10 % FBS was added to the lower chamber. Drugs were granted in the upper and lower chambers independently. Free Hol, PBAE/Hol-NPs, FA/PBAE/Hol-NPs (Hol concentrations of 0.075 μg/mL, 0.15 μg/mL and 0.3 μg/mL were set in each group, correspondingly), and a blank control group (fresh RPMI-1640 with 1% FBS) was maintained (n = 3). The cells at the bottom edge of the culture chamber were colored in crystal violet and pictured in the microscope for 24 h after cultivation. The upper side of the staining chamber was then lightly rinsed to removal of residual cells and the chamber air-dried and laundered with 33 % acetic acid (w/v), lastly the optical density (OD) at 570 nm of the eluate was taken. The upper and bottom cells of the control set the meaningful OD value to 100 %. The cell migration rate (%) was counted as below.

$$\text{Cell migration } (\%) = \frac{\text{OD}_{\text{test}}}{\text{OD}_{\text{control}}} \times 100\% \quad (3)$$

To conduct wound healing analysis, 4T1 cells were inserted in 24-well panels and incubated at a density of 3×10^5/well for 24 h. Subsequently, various Hol formulations were added into the wells. Upon incubation for 0, 12 and 24 h, the cells were visualized under an upside-down flourescent microscope (Olympus, IX-71), and the results recorded and processed with Image J.

2.12. Transwell invasion assay

Regarding the invasion assay, the cells were handled in the following manner as in the migration assay. In additional, 20 μL of Matrigel (0.5 mg/mL, diluted with serum-free RPMI1640 medium) was incorporated into Transwell chambers (the above-mentioned operation shall be performed under ice bath terms), and diluted substrate gels were then cultured in a 37 °C, 5% CO_2 cell incubator for 1 h. Likewise, the cell invasion rate (%) was determined as follows.

$$\text{Cell invasion } (\%) = \frac{\text{OD}_{\text{test}}}{\text{OD}_{\text{control}}} \times 100\% \quad (4)$$

2.13. In vivo biodistribution of DiR-loaded LPHNs

Tumor patterns were set up by the subcutaneous injection of 1×10^5 4T1 cells into the right side of Balb/c mice. 7 days later, Balb/c mouse-raw mice with a tumor volume of approximately 200 mm^3 were given FA/PBAE/DiR-NPs, PBAE/DiR-NPs, or free DiR (equivalent to a dosage of 0.5 mg/kg DiR) intravenously. The mice underwent visual imaging optically for various times while being anesthetized with IVIS imaging system (FX PRO, Carestream Health, Toronto, Canada). Hereafter, mice were slain 24 h after injection, major organs (spleen, heart, lung, kidney, liver) and tumors extracted for fluorescence images.

2.14. In vivo anti-cancer efficacy

4T1 tumor-bearing mice were reconstituted as described in the protocol above. When tumor growth was monitored up to 200 mm^3, the mice were divided at random into 4 groups (n = 5): normal Saline, free Hol group, PBAE/Hol-NPs group and FA/PBAE/Hol-NPs group, where the equivalent dose of Hol was at 15 mg/kg every two days for five treatments in total. The tumor volume and body weight of the mice were then monitored at intervals of one day. The tumor volume and inhibition rate (IR) of the mice were further assessed using formulas (5) and (6).

$$\text{V} = \frac{(\text{length}) \times (\text{width})^2}{2} \quad (5)$$

$$\text{IR} = \left(1 - \frac{\text{W}_t}{\text{W}_c}\right) \times 100\% \quad (6)$$

Where w_t and w_c were the average tumor weights of the test and control groups.

2.15. In vivo therapy effect of lung metastasis

4T1 cells were inoculated into the tail vein of Balb/c mice (female, 6–8 weeks old, 15−20 g), and the experimental metastasis model was established with 1×10^5 cells per mouse. Mice were then randomized into 4 groups (n = 5) after 7 days, and the administration regimen was the same as “2.14”. The lungs were taken after 21 days implantation.

2.16. Histological studies

For the acquired lungs, metastatic nodules were enumerated to gauge the anti-metastatic treatment efficacy of respective groups. In the case of tumors and major organs including heart, liver, spleen, lung and kidney, fixed sections would be prepared and stained with hematoxylin-eosin (H&E). Due to high expression of two matrix metalloproteinases, MMP-2 and MMP-9, in breast cancer metastasis is intimately related, fluorescent staining of lungs was conducted also with MMP-2 and MMP-9 antibodies. TUNEL of tumors was also observed for apoptosis in all groups.

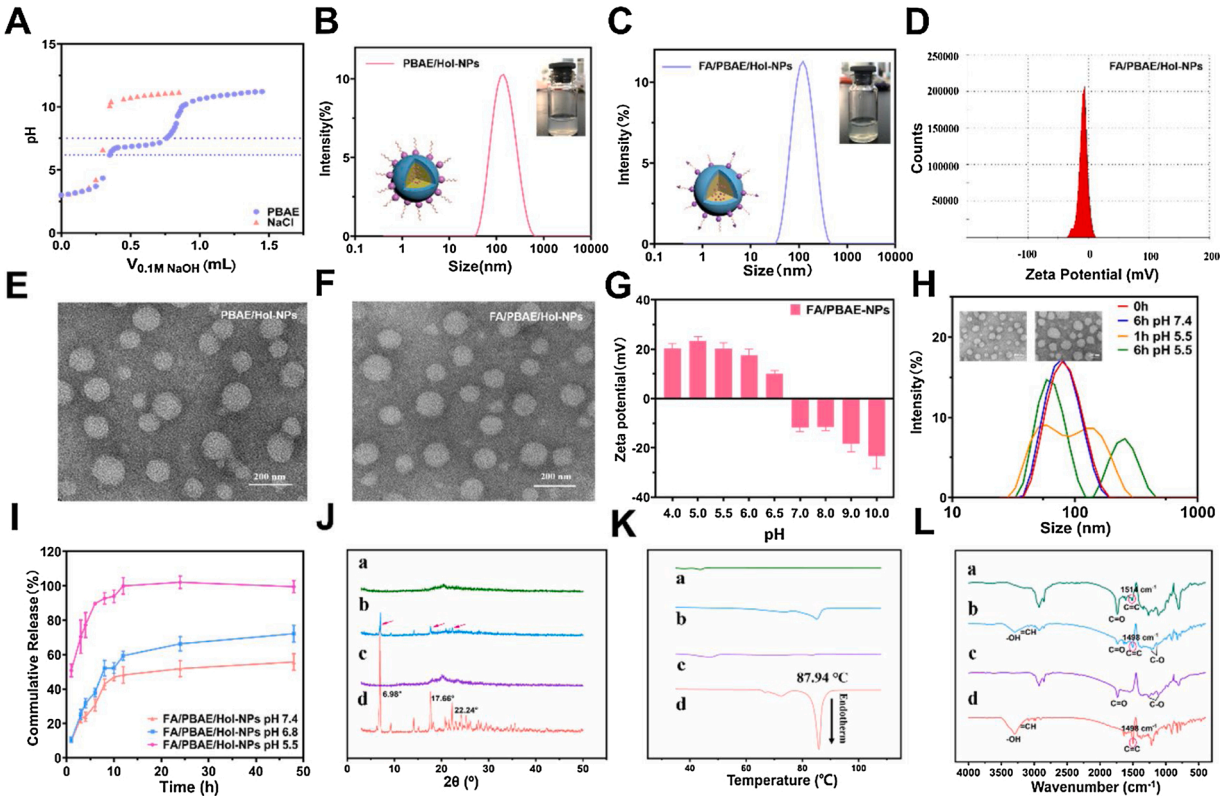

Fig. 1. (A) PBAE titration curves; (B-F) Particle size distributions, appearance, schematic diagrams, Zeta potential and TEM images of PBAE/Hol-NPs and FA/PBAE/Hol-NPs; (G) Zeta potential and (H) Particle size change of the blank LPHNs by DLS after incubation at different pH and TEM images of blank LPHNs incubated at pH 7.4 (left) and 5.5 (right) for 6 h (scale bar 200 nm); (I) *In vitro* Hol release profiling of FA/PBAE/Hol-NPs from diverse pH values; (J-L) XRD images, DSC plot and FTIR spectra of the samples (a) the Hol-loaded LPHNs; (b) the physical mixture of Hol and blank LPHNs; (c) the blank LPHNs; (d) the free Hol.

Table 1
Characterization of PBAE/Hol-NPs and FA/PBAE/Hol-NPs.

Sample (n = 3)	Size(nm)	Zeta potential (mV)	PDI	EE (%)	DL (%)
PBAE/Hol-NPs	105.3 ± 3.2	−6.8 ± 2.6	0.24 ± 0.01	78.1 ± 2.5	11.4 ± 2.6
FA/PBAE/Hol-NPs	116.4 ± 5.1	−8.9 ± 3.7	0.21 ± 0.02	75.2 ± 3.8	10.9 ± 1.4

2.17. Statistical analysis

For all trials, all tests were performed at least 3 times. Data were displayed as mean ± standard deviation (SD). Outcomes were presented using a Student's *t*-test and a multiple-group one-way ANOVA. The discrepancy was statistically meaningful and was established as $*p \leq 0.05$.

3. Results and discussion

3.1. Synthesis and characterization of PBAE

The one-pot synthesis of amphiphilic copolymers by Michael additions has distinct merits in terms of gentle reaction conditions and convenience in inducing diverse functionality groups and ligands [29]. The synthetic route of PBAE was elucidated entirely in Fig. S1, which was optimized by ^{1}H NMR Fig. S2.

The pKb value of the polymer, namely the inflection point, was calculated from the derivative value of the titration curve by acid-base titration experiments. As illustrated in Fig. 1A, the pKb value of PBAE was computed to be 6.5 which is close to the pH value of lysosome.

3.2. Physicochemical characterization of LPHNs

The hydrodynamic dimensions of PBAE/Hol-NPs and FA/PBAE/Hol-NPs were 105.3 ± 3.2 nm and 116.4 ± 5.1 nm (Fig. 1B, C), consistent with those in the TEM plots (Fig. 1E, F). And the zeta potential was - 6.8 ± 2.6 mV and - 8.9 ± 3.7 mV (Fig. 1D). The DL% and EE% of FA/PBAE/Hol-NPs were 10.9 ± 1.4 % and 75.2 ± 3.8 % (Table 1). DLS measurements at varying time points in PBS (pH 7.4) (Fig. S3) or FBS (10 %) indicated promising stabilities of FA/PBAE/Hol-NPs (Fig. S4).

3.3. Surface charge transition and pH reactivity

The Zeta potential of FA/PBAE-NPs reversed from + 20.4 mV to - 23.4 mV as the surrounding pH changed from 4 to 10 after incubation for 1 h (Fig. 1G). In addition, with the decrease of the surrounding pH value, the positive charge of FA/PBAE-NPs further increases. Fig. 1H shows that as time progressed, FA/PBAE-NPs shows a constant average size of 91.3 nm at pH 7.4. When the surrounding pH decreased to 5.5, FA/PBAE-NPs had a distinct swelling, and with the extension of culture time, the swelling became more pronounced, and there was a multi-peak phenomenon in distribution. In conclusion, the charge reversal and particle size change of FA/PBAE-NPs are mainly caused by PBAE tertiary amine matrization (Fig. S5), and its pKb is negatively charged FA/PBAE-NPs under to physiological terms are more stabilized in the circulating blood and have fewer non-specific interactions for serum proteins.

3.4. In vitro releasing profiles

A variety of pH were adopted to imitate natural biological organisms and tumor microenvironment conditions. *In vitro* Hol release profiles from Hol-loaded LPHNs were illustrated in Fig. 1I, FA/PBAE/Hol-NPs

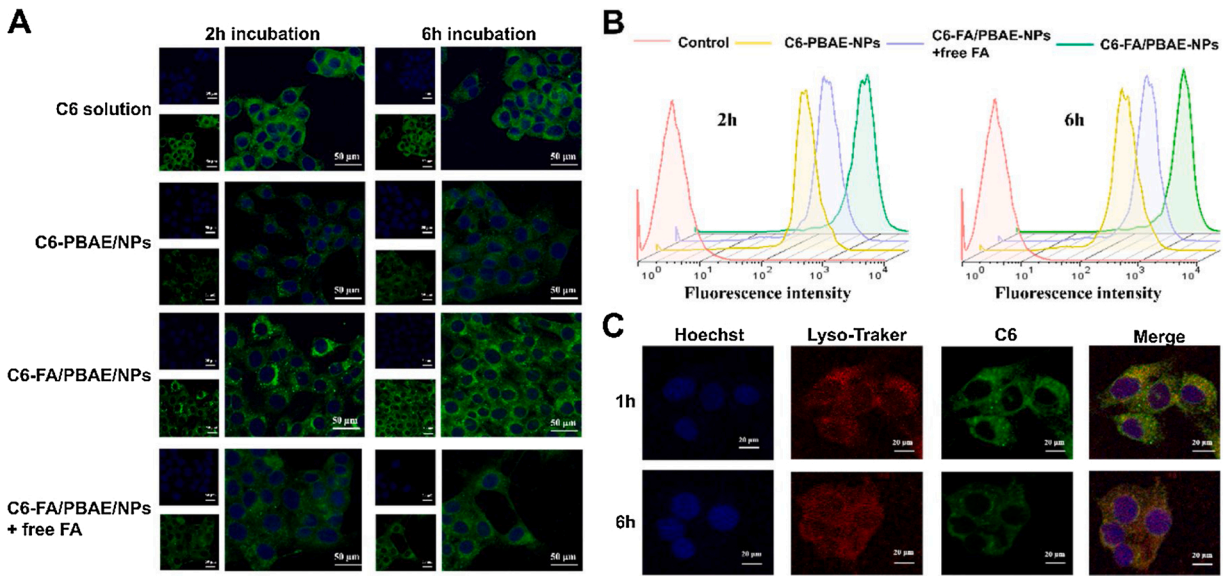

Fig. 2. (A) Convergent microscopic images of C6-loaded LPHNs after 2 h and 6 h (The scale bar is 50 μm); (B) Analysis of the fluorescence intensity *via* flow cytometry; (C) CLSM pictures of C6-FA/PBAE-NPs from 4T1 cells upon 1 h and 6 h incubation. Lyso Tracker™ Red (Red) for staining lysosomes was employed. The scale bar is 20 μm.

had a release of only 42.7 % Hol in pH 7.4 and 52.1 % Hol in pH 6.8 after 8 h. Additionally, a noticeably and dramatically higher pH release was in the case of pH 5.5 and the release count hit 92.6 % in 8 h. The release of this pH-sensitive FA/PBAE/Hol-NPs will enhance the internalization of the drug and effectively inhibit the proliferation of cancer cells, due to the on-demand release of Hol in different physiological environments.

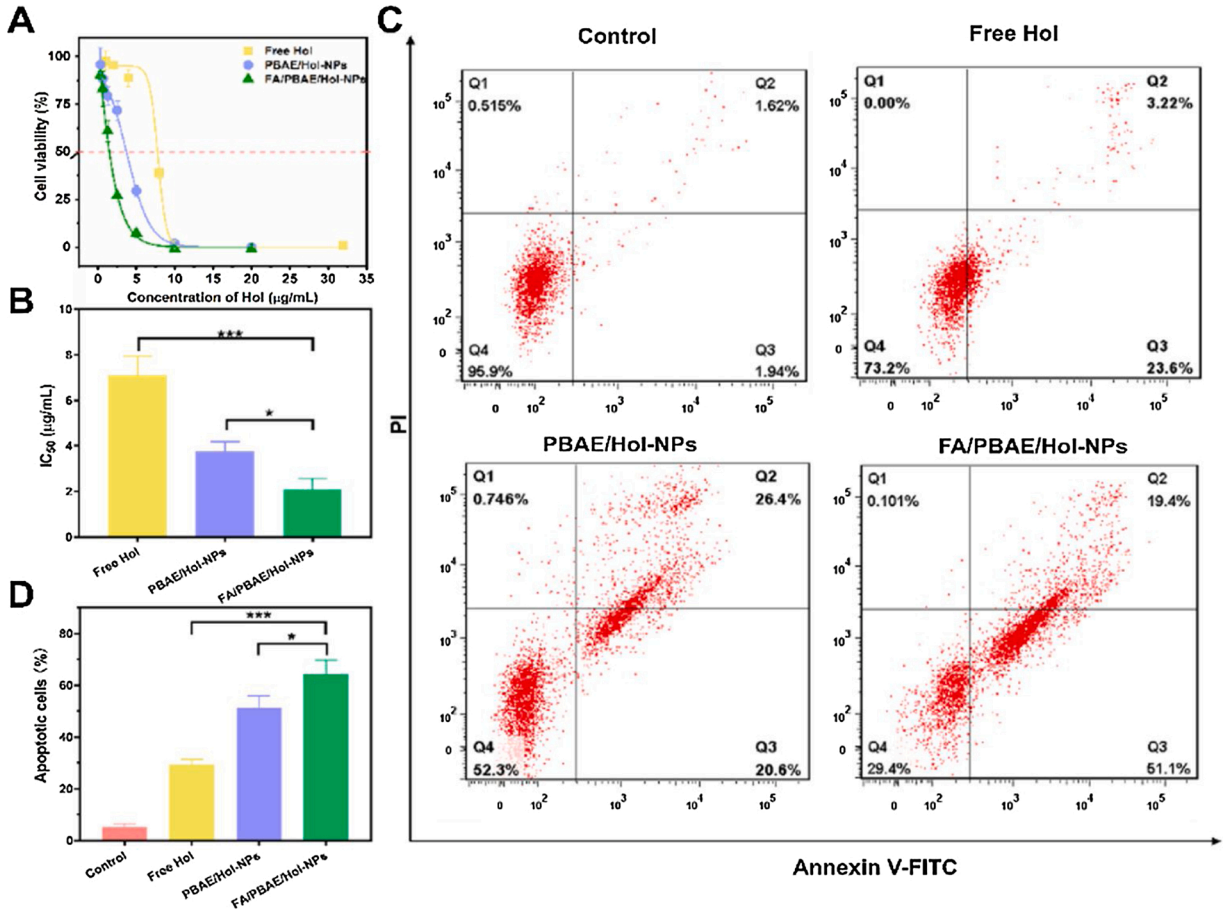

Fig. 3. 4T1 *in vitro* cellular toxicities and cell apoptosis assessment. (A) Cell viability of Hol preparations. (B) IC_{50} values (C) Flow cytometry analysis for the apoptosis of Hol preparations. (D) Quantification analysis of apoptotic/necrotic cell populations. $^{*}p < 0.05$, $^{***}p < 0.001$.

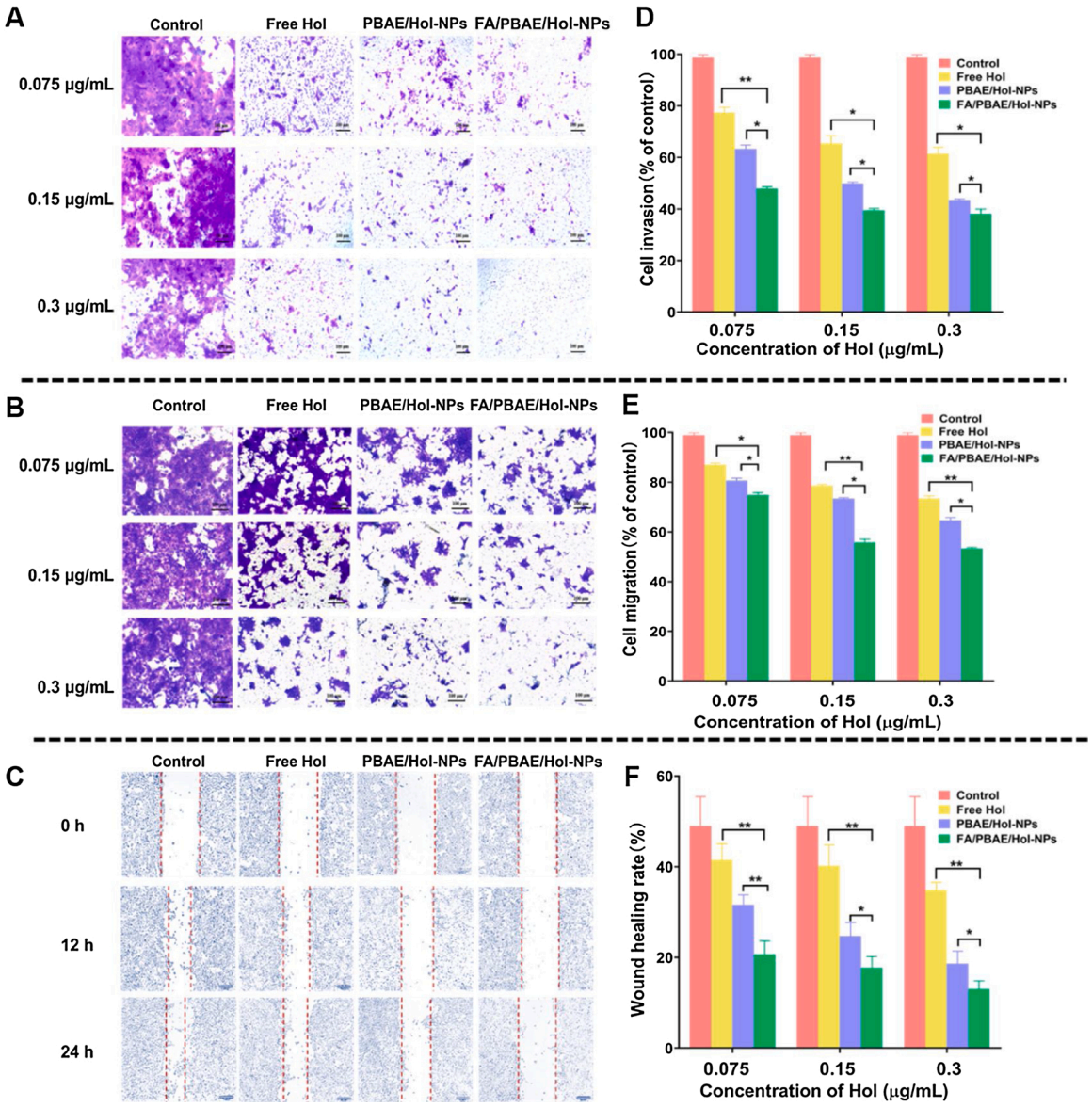

Fig. 4. Inhibitory properties of Hol-loaded LPHNs on the migratory and invasive capabilities of 4T1 cells *in vitro*. Typical images of (A) Invasion (B) Transwell migration and (C) Wound healing migration assessments. Quantitative profiling of (D) Invasion (E) Transwell migration test. (F) Wound healing. $*p < 0.05$, $**p < 0.01$. The scale bar is 100 μm.

3.5. Physicochemical properties characterization of FA/PBAE/Hol-NPs

In Fig. 1J, the XRD patterns of the free Hol (d curve) displayed intensive peaks at 2θ of 6.98°, 17.66° and 22.24°, and lots of tiny peaks were in the range of within the range of 3°-50°. The classic crystalline peak of Hol is nevertheless seen within the model of PM (b curve), despite the diminished intensity. Yet, not visible in the Hol-loaded LPHNs (a curve).

In Fig. 1K, free Hol has a marked thermal absorbtion peak at 87.94 °C (d curve), represents the Hol melting point. In the DSC diagram of Hol-loaded LPHNs (a curve), no sharp peak was detected at 87.94 °C.

In Fig. 1L, the FTIR spectra of free Hol (d curve), the 3306 cm^{-1} peak is dedicated to the −OH vibration and the 1637 cm^{-1} peak is attributed to the alkene CC═ vibration. The intensive belt at 1498 cm^{-1} falls into the CC═ aromatic group of stretches. For the blank LPHNs (c curve), the peak at 1738 cm^{-1} was attributed to the C═O stretching vibration of the ester, and the peak at 1273 cm^{-1} and 1095 $cm^{-1}$was ascribed to the C—O stretching vibration of the carboxyl. However, from the spectrum of the Hol-loaded LPHNs (a curve), all absorption peaks of Hol almost disappear. Only observed the C═C aromatic stretched bands of Hol, which went up from 1498 cm^{-1} into 1514 cm^{-1}. Combined with XRD, DSC and FTIR, we can directly find that Hol exists in LPHNs in the form of partial or amorphous, which is helpful to facilitate the dissolution and bioavailability to the drug.

3.6. In vitro cellular uptake and distribution of Hol-loaded NPs

In Fig. 2A, after incubation of 4 h, the cellular uptake of C6-LPHNs was temporally dependent obviously. The uptake of C6-FA/PBAE-NPs was the strongest at all time points, which was benefited from the effective endocytosis mediated by FA. Furthermore, competitive inhibition of free FA incubation inhibited the uptake of C6-FA/PBAE-NPs, providing further support that FA-modified LPHNs may facilitate intracellular uptake by FR-α mediated endocytosis.

Results of the quantitative flow cytometry analysis, indicated that cells incubated with C6-FA/PBAE-NPs exhibited a higher uptake than C6-PBAE-NPs and C6 solution (Figs. 2B, S6). In a further, the uptake of C6-FA/PBAE-NPs was markedly decreased when FA were saturated.

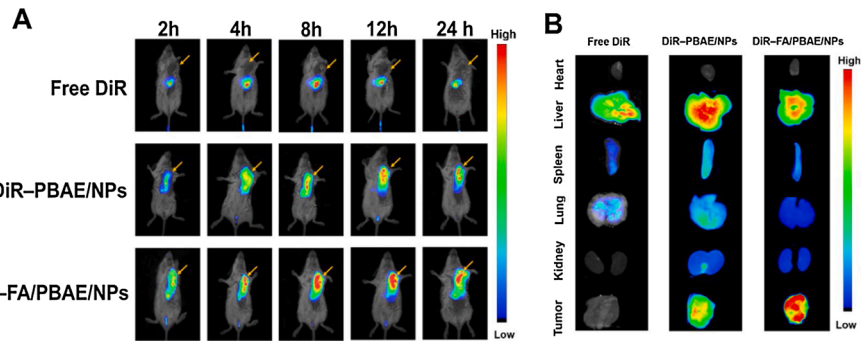

Fig. 5. *In situ* tracking of DiR-labeled LPHNs to breast 4T1 tumor. (A) *In vivo* fluorescence images; (B) *In vitro* fluorescence imaging of autopsied tumors and organ at 24 h post-injection.

This is in accordance with the confocal results. Moreover, the fluorescence of C6-LPHNs gradually increased with time.

To detect the intracellular transit of drug-laden NPs, the intracellular administration efficiency of C6-LPHNs was captured by CLSM. In Fig. 2C, the yellow fluorescence of C6-PBAE-NPs and C6-FA/PBAE-NPs was intense upon incubation time of 1 h, which meant that the majority of C6-loaded NPs were colocalized with endo/lysosomes. Yellow fluorescence diminished and green fluorescence dispersed outward with the extension of the cultivation period to 6 h. Combined with the cellular uptake results above, it was indicated that endo/lysosomal escape of C6-PBAE-NPs and C6-FA/PBAE-NPs occurred, enabling effective and speedy drug discharge, which was probably resulted from the protonation of PBAE by the cells under endo/lysosomal acidic conditions following uptake.

3.7. *In vitro cytotoxicity studies and apoptotic rate*

Cellular toxicity evaluated by MTT detection of 4T1 cells. When PBAE concentration is 200 μg/mL, the cell survival rate of the blank vector is still more than 75 % (Fig. S7). Hol formulations including both free Hol and Hol-loaded LPHNs exhibited strong cytotoxicity in a concentration-dependent manner. The IC_{50} of free Hol, PBAE/Hol-NPs and FA/PBAE/Hol-NPs were 7.08 μg/mL, 3.75 μg/mL and 2.07 μg/mL (Fig. 3A-B). The Hol loaded LPHNs showed stronger cytotoxicity than free Hol, which may be due to the increased internalization of NPs with positive charge in the tumor microenvironment, and then into the cell caused by tertiary amine protonation of PBAE, the drug quickly escaped from the lysosome. In addition, 4T1 cells showed that the preparation with FA target had the strongest cytotoxicity because of overexpressed FR-α on the surface.

Apoptosis is a procedural cell death in multicellular organisms and an influential tactic for managing cancer prognosis. The apoptotic cell percentages (Q2 + Q3) were 5.15 %, 29.16 %, 51.38 % and 64.43 % for Control, free Hol, PBAE/Hol-NPs and FA/PBAE/Hol-NPs, separately (Fig. 3C-D). The findings of apoptosis were in line with cytotoxicity, suggesting that FA/PBAE/Hol-NPs had the most capability to evoke apoptosis in 4T1 cells.

3.8. *4T1 cell invasion assignment*

Tumor metastases are processes in which the extracellular matrix of a tumor is destroyed and then invades the vessels, involving at least both invasion and migration phases [30]. Cell invasion is a prerequisite for initiating tumor metastasis. Firstly, it is notable to ensure that the choice of drug concentration should ensure that the cell survival rate is higher than 80 %. Then, combined with the results of cytotoxicity test, three concentrations of low (0.075 μg/mL), medium (0.15 μg/mL), high (0.3 μg/mL) were selected to investigate the ability of cell invasion and migration, which is expected to be more in-depth investigation and the ability of magnolol drug-loaded preparation to inhibit breast cancer metastasis, and provide more valuable reference for future research.

The invasive ability of 4T1 cells passing through Matrigel gel was markedly after treatment with different drug concentrations (Fig. 4D). Excitingly, when the drug concentration decreased to 0.075 μg/mL (75 ng/mL), compared with free Hol (77.4 %) and PBAE/Hol-NPs (63.3 %), the anti-invasion ability of FA/PBAE/Hol-NPs was greatly increased, about 47.9 %, indicating that FA/PBAE/Hol-NPs can well inhibit cell invasion at even very lower drug concentrations. This superiority was reinforced by a fluorescent microscopic picture of cells passed across the stroma coating and attached to the lower side of the membranes (Fig. 4A). All the results showed that FA/PBAE/Hol-NPs alone significantly inhibited the invasion of the 4T1 cells (Fig. 4B).

3.9. *4T1 cell migration assessment*

Aiming to qualitatively and quantitatively study whether Hol-loaded LPHNs can inhibit the migration of 4T1 cells, the same concentrations were selected to investigate migration ability. The inhibitory impact of the application group against 4T1 cell migration was also found in a concentrate-dependent mode (Fig. 4E). Concordant with the invasion results, there was a remarkable difference in the inhibitory effect of varying concentrations of Hol-LPHNs on the migration of 4T1 cells. The same image of cells dyed in crystal violet across the membrane and adhering to the bottom of the membrane also shows above messages (Fig. 4B). The results of wound healing experiment further confirmed the inhibitory effect of drug-loaded preparation on the migration of 4T1 cells (Fig. 4C, F). Taken together, cell migration and scratch healing assays suggest that FA/PBAE/Hol-NPs can be used to prevent migration of breast cancer cells.

3.10. *In vivo bio-distribution research*

A difference in the targeting capacity of DiR-labeled LPHNs were appraised by fluorescence imaging and *in vivo* histological distribution (DiR was used as a fluorescence dye). As illustrated by Fig. 5A, among the free DiR group, hepatic fluorescence increasing with time, reaching a peak at 8 h and then declining at a slow pace. The fluorescence intensity of tumor tissue in PBAE/DiR-NPs group and FA/PBAE/DiR-NPs group increased steadily after 2 h–12 h, while FA/PBAE/DiR-NPs group was the strongest in the overall trial. *Ex vivo* fluorescence imagery of the resected tumor reinforced the findings derived from *in vivo* imagery (Fig. 5B). The above results intuitively show that drug-loaded NPs with FA and good serum stability can an extend the cycle period and, even importantly, that pH-induced charge reversal can enhance the uptake in tumor tissues after accumulated.

3.11. *In vivo anticancer efficacy*

Two models, BALB/c mouse subcutaneous ectopic tumor and a pulmonary metastatic breast cancer model, have been constructed to

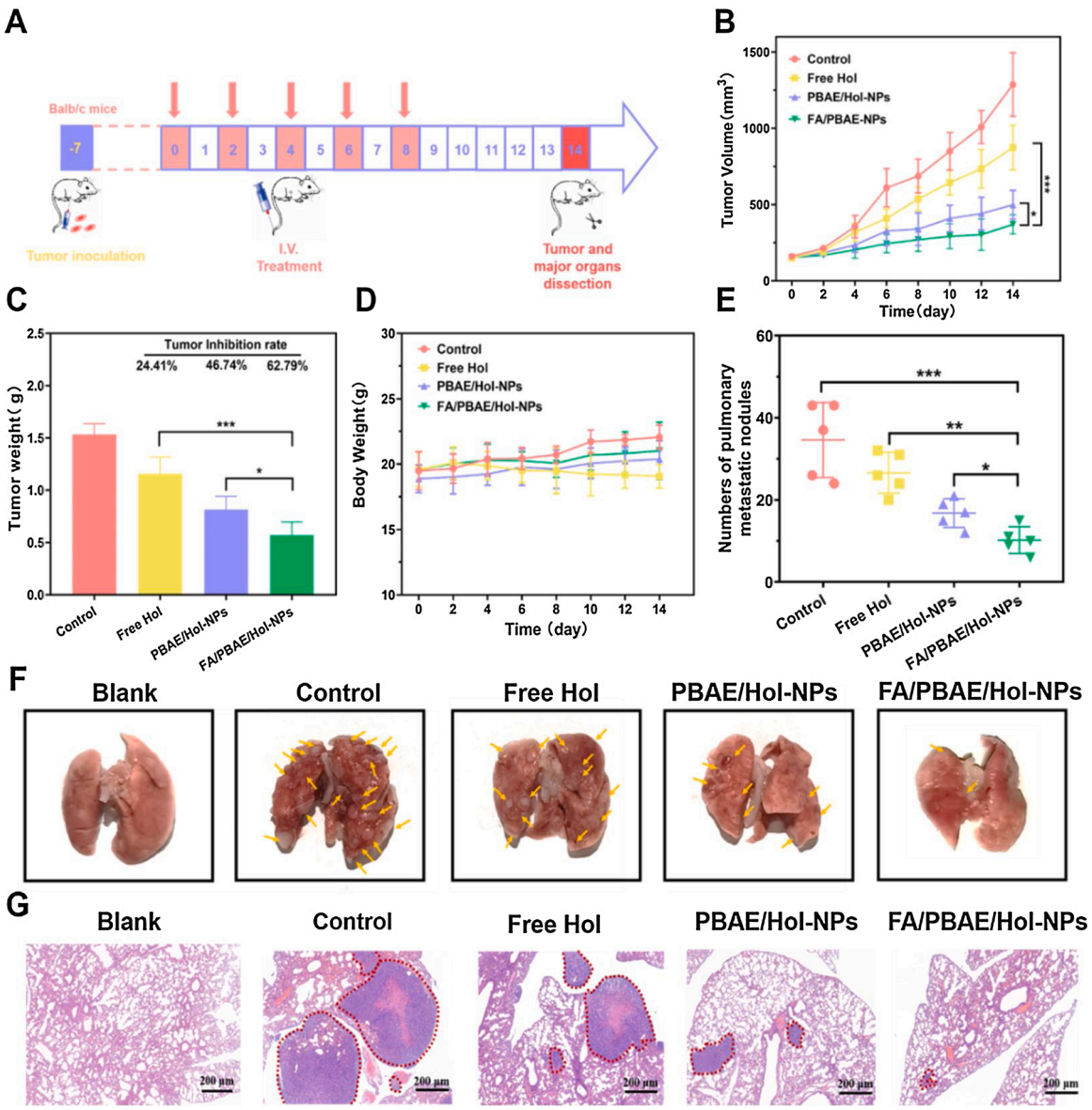

Fig. 6. (A) A schematic diagram showing the design of experiments for FA/PBAE/Hol-NPs to suppress tumor and metastasis in the lung is illustrated. *In vivo* anti-neoplastic efficiencies and toxicity profiles of mice bearing 4T1 tumors trained with Hol-loaded-NPs. (B) Variation in tumor volume, (C) Mass changes of resected tumors, (D) Net weight loss of mice; *In vivo* evaluating the anti-cancer effectiveness of a pulmonary metastatic breast cancer phantom. (E) Numbers of lung metastatic lesions. (F) Photographs and (G) H&E staining in pulmonary metastases sites. The scale bar is 200 μm. (n = 5, error bars for ± SD).

evaluation the antitumor and anti-metastatic effects of FA/PBAE/Hol-NPs. Different preparations were administered *via* tail vein every 2 days for a total of 5 treatments to investigate their anti-tumor properties (Fig. 6A). Free Hol displayed the mildest tumor growth inhibition (IR = 24.4 %), while chemotherapy with PBAE/Hol-NPs (IR = 46.7 %) revealed a medium degree of tumor growth inhibition. Remarkably, FA/PBAE/Hol-NPs presented the most intense tumor suppressive therapeutic efficacy (IR = 62.8 %), with near complete inhibition of tumor growth within 15 days of medical treatment. At the termination of the experiment, the rats were expended and the primary organs and tumors were autopsied. The outcomes of tumor mass as well as tumor suppression rate gave additional validation of the remarkable therapeutic effect of FA/PBAE/Hol-NPs compared to other treatments (Fig. 6B, C). Equally important, systemic toxicity needs to be evaluated for safety, even though the drug delivery system offers even if the delivery system has a promising therapeutic profile. Regarding security ratings, none of the therapy groups were identified as having noticeable body mass loss (Fig. 6D).

Recent studies have revealed that the usage of Hol as a monodrug demands a higher dose (=50 mg/kg) to exert remarkable activity against cancer in metastatic breast cancer [31]. Nevertheless, in this present work, encapsulation of Hol into FA/PBAE-lipid polymer hybrid nanoparticles led to a pronounced enhancement of the therapeutic effect of Hol *in vivo* uniformly in spite of a low dosage (15 mg/kg), which was corroborated by a favorable tumor volumetric and mass suppression.

3.12. *In vivo assessment of metastasis resistance*

The curative efficacy of FA/PBAE/Hol-NPs was proven in a pulmonary metastasis pattern of breast cancer. Following treatment with varying therapies, organ lungs were gathered from the respective groups and examined for well-established lung metastases. As illustrated in Fig. 6E, there were approximately 54 lesions on the lungs (Saline group), whereas all remaining treatments revealed a reduction in lung metastases. Metastases in the FA/PBAE/Hol-NPs group were noticeably inferior to those in the Saline group (84.3 %), the free Hol group (46.1 %)

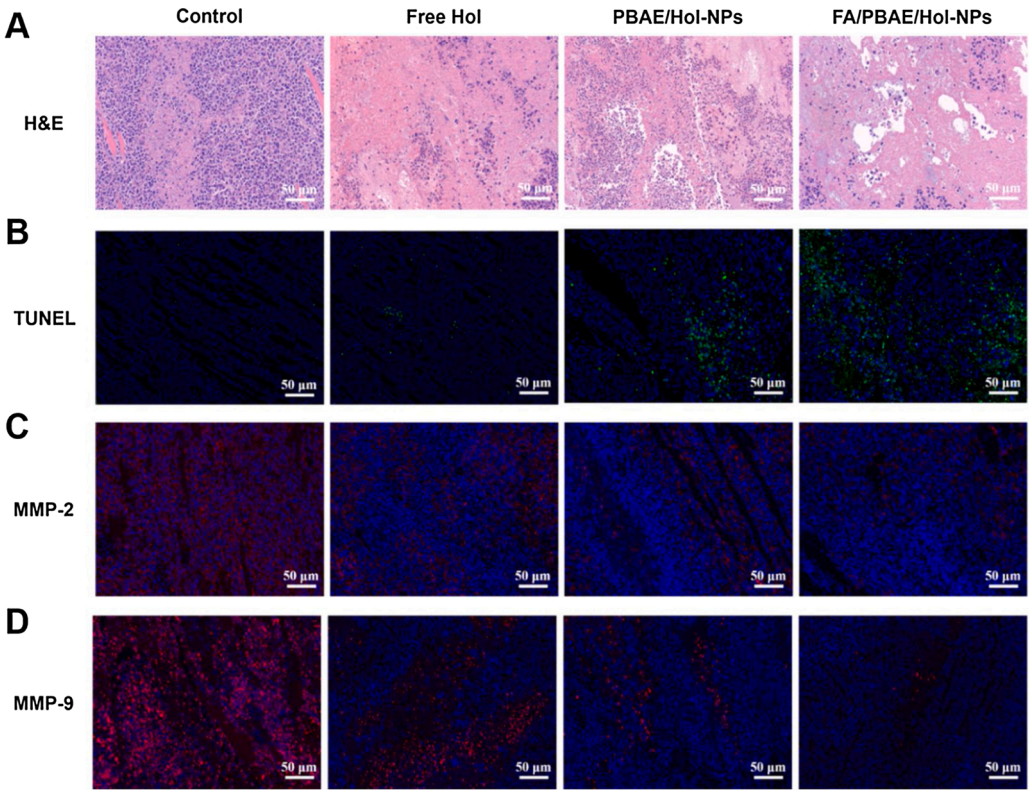

Fig. 7. Immunohistochemistry evaluation of tumor tissues (A) H&E and (B) TUNEL. Assessing tumor invasion and metastasis in lung slides by (C) MMP-2 and (D) MMP-9 immunofluorescence dyeing in a lung metastasis model, scale bar =50 μm.

and PBAE/Hol-NPs group (69.2 %). Both whole lung observation and HE staining examination showed negligible lung metastasis in the FA/PBAE/Hol-NPs treated group of mice (Fig. 6F, G), which may be explained by the increased uptake at the target site and effective drug release. As such, FA/PBAE/Hol-NPs could be serve as an excellent nano platform, which is likely owing to the highly dispersible, limited size and poor devascularization of nano-targeted chemotherapy agents and accessible to metastatic tumor sites.

3.13. Histology studies

H&E staining indicated no visible lesions in the major organs of all groups, confirming a well-established biocompatibility (Fig. S8). In the same vein, the findings (Fig. 7A, B) strongly showing numerous apoptotic areas in tumors of FA/PBAE/Hol-NPs group, further justifying its excellent *in vivo* antitumor efficacy and diminished whole-body toxicity. Notably, both MMP-2 and MMP-9 have been implicated in lung metastasis in breast cancer [2,32], which could degrade type IV collagen in the basement membrane, facilitating tumor cell proliferation, disrupting the basement membrane barrier and adding to tumor cell metastasis. Consequently, FA/PBAE/Hol-NPs can seemingly block MMPs pathway by repression the exposure of two metastasis-related matrix metalloproteinases (Fig. 7C, D).

4. Conclusion

A pH-responsive lipid polymer hybrid nanoparticle, in which Hol was encapsulated, was fabricated for accurate delivery of agents for the diagnosis and treatment of breast cancer and lung metastases. After *i.v.*, the Hol-loaded LPHNs amassed at the tumor region. By provoking the protonation of tertiary amines in the tumor microenvironment, the rupture of LPHNs enables the targeting of its cargo for vehicle transport and controllable release of drugs. Also, in comparing with PBAE/Hol-NPs, FA/PBAE/Hol-NPs had marked endocytic uptake efficacy, cell toxicity and pre-apoptotic in the presence of FR-α mediated endocytosis. Excitingly, FA/PBAE/Hol-NPs treatment not only elicited an effective tumor suppression effect, but also repressed the MMPs pathway linked to metastasis, thus fostered pulmonary metastasis. Moreover, it also possessed promising biocompatible between major organs. As such, FA/PBAE/Hol-NPs are likely to hold substantial potential to combat primary breast cancer as well as lung metastasis.

CRediT authorship contribution statement

Hongyan Zhang: Writing - review & editing, Writing - original draft, Data curation, Conceptualization. **Ji Li:** Validation, Formal analysis. **Rong Yuan:** Investigation. **Yufen Li:** Supervision, Validation. **Yue Zhang:** Supervision, Methodology. **Xiaoyun Hu:** Investigation. **Jiqiang Qu:** Investigation. **Yu Chen:** Software. **Zheran Wang:** Visualization, Software. **Mingyu Xia:** Project administration, Supervision. **Dongkai Wang:** Resources, Funding acquisition.

Declaration of Competing Interest

The authors report no declarations of interest.

Appendix A. Supplementary data

Supplementary material related to this article can be found, in the online version, at doi:https://doi.org/10.1016/j.colsurfb.2021.112008.

References

[1] L.T. Jin, B.C. Han, E. Siegel, Y.K. Cui, A. Giuliano, X.J. Cui, Breast cancer lung metastasis: molecular biology and therapeutic implications, Cancer Biol. Ther. 19 (10) (2018) 858–868.
[2] L. Luo, F. Xu, H. Peng, Y. Luo, X. Tian, G. Battaglia, H. Zhang, Q. Gong, Z. Gu, K. Luo, Stimuli-responsive polymeric prodrug-based nanomedicine delivering

nifuroxazide and doxorubicin against primary breast cancer and pulmonary metastasis, J. Control. Release 318 (2020) 124–135.
[3] M. Yousefi, R. Nosrati, A. Salmaninejad, S. Dehghani, A. Shahryari, A. Saberi, Organ-specific metastasis of breast cancer: molecular and cellular mechanisms underlying lung metastasis, Cell. Oncol. 41 (2) (2018) 123–140.
[4] Y. Chen, H. Gu, D.S. Zhang, F. Li, T. Liu, W. Xia, Highly effective inhibition of lung cancer growth and metastasis by systemic delivery of siRNA via multimodal mesoporous silica-based nanocarrier, Biomaterials 35 (38) (2014) 10058–10069.
[5] N. Yang, Y. Jiang, H. Zhang, B. Sun, C. Hou, J. Zheng, Y. Liu, P. Zuo, Active targeting docetaxel-PLA nanoparticles eradicate circulating lung cancer stem-like cells and inhibit liver metastasis, Mol. Pharm. 12 (1) (2015) 232–239.
[6] J. Shi, P.W. Kantoff, R. Wooster, O.C. Farokhzad, Cancer nanomedicine: progress, challenges and opportunities, Nat. Rev. Cancer 17 (1) (2017) 20–37.
[7] X. Gu, Y. Gao, P. Wang, L. Wang, H. Peng, Y. He, Y. Liu, N. Feng, Nano-delivery systems focused on tumor microenvironment regulation and biomimetic strategies for treatment of breast cancer metastasis, J. Control. Release 333 (2021) 374–390.
[8] S. Lv, Z. Tang, M. Li, J. Lin, W. Song, H. Liu, Y. Huang, Y. Zhang, X. Chen, Co-delivery of doxorubicin and paclitaxel by PEG-polypeptide nanovehicle for the treatment of non-small cell lung cancer, Biomaterials 35 (23) (2014) 6118–6129.
[9] J. Wang, D. Liu, S. Guan, W. Zhu, L. Fan, Q. Zhang, D. Cai, Hyaluronic acid-modified liposomal honokiol nanocarrier: enhance anti-metastasis and antitumor efficacy against breast cancer, Carbohydr. Polym. 235 (2020), 115981.
[10] L. Luo, J. Nong Wang, L.D. Kong, Q.G. Jiang, R.X. Tan, Antidepressant effects of Banxia Houpu decoction, a traditional Chinese medicinal empirical formula, J. Ethnopharmacol. 73 (1–2) (2000) 277–281.
[11] A. Sugaya, T. Tsuda, T. Obuchi, E. Sugaya, Effect of Chinese herbal medicine "Hange-Koboku-To" on laryngeal reflex of cats and in other pharmacological tests, Planta Med. 47 (1) (1983) 59–62.
[12] B. Wu, S.H. Fu, H. Tang, K. Chen, Q. Zhang, A.H. Peng, H.Y. Ye, X.J. Cheng, M. Lian, Z.L. Wang, L.J. Chen, Design, synthesis and antibacterial evaluation of honokiol derivatives, Bioorg. Med. Chem. Lett. 28 (4) (2018) 834–838.
[13] S.Z. Chen, Research progress in anticancer effects and molecular targets of honokiol in experimental therapy, Yao Xue Xue Bao 51 (2) (2016) 202–207.
[14] S.K. Katiyar, Emerging phytochemicals for the prevention and treatment of head and neck cancer, Molecules 21 (12) (2016).
[15] T.Q. Lang, X.Y. Dong, Y. Huang, W. Ran, Q. Yin, P.C. Zhang, Z.W. Zhang, H.J. Yu, Y.P. Li, Ly6C(hi) monocytes delivering pH-Sensitive micelle loading paclitaxel improve targeting therapy of metastatic breast cancer, Adv. Funct. Mater. 27 (26) (2017).
[16] M.G. Vander Heiden, L.C. Cantley, C.B. Thompson, Understanding the Warburg effect: the metabolic requirements of cell proliferation, Science 324 (5930) (2009) 1029–1033.
[17] F. Li, W.L. Chen, B.G. You, Y. Liu, S.D. Yang, Z.Q. Yuan, W.J. Zhu, J.Z. Li, C.X. Qu, Y.J. Zhou, X.F. Zhou, C. Liu, X.N. Zhang, Enhanced cellular internalization and on-demand intracellular release of doxorubicin by stepwise pH-/reduction-responsive nanoparticles, ACS Appl. Mater. Interfaces 8 (47) (2016) 32146–32158.
[18] P. Yu, H. Yu, C. Guo, Z. Cui, X. Chen, Q. Yin, P. Zhang, X. Yang, H. Cui, Y. Li, Reversal of doxorubicin resistance in breast cancer by mitochondria-targeted pH-responsive micelles, Acta Biomater. 14 (2015) 115–124.
[19] T. Wang, D. Wang, H. Yu, M. Wang, J. Liu, B. Feng, F. Zhou, Q. Yin, Z. Zhang, Y. Huang, Y. Li, Intracellularly acid-switchable multifunctional micelles for combinational photo/chemotherapy of the drug-resistant tumor, ACS Nano 10 (3) (2016) 3496–3508.
[20] J. Gao, W.Q. Wang, H.J. Yu, Acid-activatable polymeric drug delivery systems for cancer therapy, Acta Polym. Sin. 50 (11) (2019) 1156–1166.
[21] X. Gao, Z. Jin, X. Tan, C. Zhang, C. Zou, W. Zhang, J. Ding, B.C. Das, K. Severinov, I.I. Hitzeroth, P.R. Debata, D. He, X. Ma, X. Tian, Q. Gao, J. Wu, R. Tian, Z. Cui, W. Fan, Z. Huang, C. Cao, Y. Bao, S. Tan, Z. Hu, Hyperbranched poly(beta-amino ester) based polyplex nanopaticles for delivery of CRISPR/Cas9 system and treatment of HPV infection associated cervical cancer, J. Control. Release 321 (2020) 654–668.
[22] C. Zhang, T. An, D. Wang, G. Wan, M. Zhang, H. Wang, S. Zhang, R. Li, X. Yang, Y. Wang, Stepwise pH-responsive nanoparticles containing charge-reversible pullulan-based shells and poly(beta-amino ester)/poly(lactic-co-glycolic acid) cores as carriers of anticancer drugs for combination therapy on hepatocellular carcinoma, J. Control. Release 226 (2016) 193–204.
[23] E. Oude Blenke, S. Mahakena, M. Fens, J. van den Dikkenberg, M. Holkers, E. Mastrobattista, Impact of chemistry and nanoformulation parameters on cellular uptake and airway distribution of RNA oligonucleotides, J. Control. Release 317 (2020) 154–165.
[24] X. Zhang, N. Liang, X. Gong, Y. Kawashima, F. Cui, S. Sun, Tumor-targeting micelles based on folic acid and alpha-tocopherol succinate conjugated hyaluronic acid for paclitaxel delivery, Colloids Surf. B Biointerfaces 177 (2019) 11–18.
[25] L. Wang, Y. Liu, J. Zhao, C. Li, Y. Zhou, J. Du, Y. Wang, *In vitro* and *in vivo* evaluation of targeting tumor with folate-based amphiphilic multifunctional stabilizer for resveratrol nanosuspensions, Colloids Surf. B Biointerfaces 160 (2017) 462–472.
[26] W. Xiao, Y. Wang, H. Zhang, Y. Liu, R. Xie, X. He, Y. Zhou, L. Liang, H. Gao, The protein corona hampers the transcytosis of transferrin-modified nanoparticles through blood-brain barrier and attenuates their targeting ability to brain tumor, Biomaterials 274 (2021), 120888.
[27] W. Xiao, H. Gao, The impact of protein corona on the behavior and targeting capability of nanoparticle-based delivery system, Int. J. Pharm. 552 (1–2) (2018) 328–339.
[28] C.F. Yang, Z.L. Xue, Y.L. Liu, J.Y. Xiao, J.R. Chen, L.J. Zhang, J.W. Guo, W.J. Lin, Delivery of anticancer drug using pH-sensitive micelles from triblock copolymer MPEG-b-PBAE-b-PLA, Mater. Sci. Eng. C-Mater. 84 (2018) 254–262.
[29] N. Peng, H. Yu, W. Yu, M. Yang, H. Chen, T. Zou, K. Deng, S. Huang, Y. Liu, Sequential-targeting nanocarriers with pH-controlled charge reversal for enhanced mitochondria-located photodynamic-immunotherapy of cancer, Acta Biomater. 105 (2020) 223–238.
[30] J.J. Bravo-Cordero, L. Hodgson, J. Condeelis, Directed cell invasion and migration during metastasis, Curr. Opin. Cell Biol. 24 (2) (2012) 277–283.
[31] W.D. Wang, Y. Shang, Y. Li, S.Z. Chen, Honokiol inhibits breast cancer cell metastasis by blocking EMT through modulation of Snail/Slug protein translation, Acta Pharmacol. Sin. 40 (9) (2019) 1219–1227.
[32] L. Szabova, K. Chrysovergis, S.S. Yamada, K. Holmbeck, MT1-MMP is required for efficient tumor dissemination in experimental metastatic disease, Oncogene Basingstoke 27 (23) (2008) 3274–3281.